

Uncovering quantum characteristics of incipient evolutions at the photosynthetic oxygen evolving complex

Pei-Ying Huo,¹ Wei-Zhou Jiang,^{1,*} Rong-Yao Yang,¹ and Xiu-Rong Zhang²

¹*School of Physics, Southeast University, Nanjing 211189, China*

²*School of Science, Jiangsu University of Science and Technology, Zhenjiang 212100, China*

Water oxidation of photosynthesis at the oxygen evolving complex (OEC) is driven by the polarization field induced by the photoelectric hole. By highlighting the role of the polarization field in reshaping the spin-orbit coupling deduced from the Dirac quantum mechanics, we reveal in this work the characteristics and underlying mechanism in the relatively simpler OEC evolutions within the states $S_0 \sim S_2$ prior to the water oxidation. The characteristic shifts of the density of states (DOS) of the electron donor Mn atom are observed in the vicinity of the Fermi surface to occur with the spin flips of Mn atoms and the change of the Mn oxidation states during the electron transfer. Notably, the spin flips of Mn atoms point to the resulting spin configuration of the next states. It is found that the electron transfer tend to stabilize the catalyst OEC itself, whereas the proton transfer pushes the evolution forward by preparing a new electron donor. Meanwhile, it shows that the Mn-O bonds around the candidate Mn atom of the electron donor undergo characteristic changes in the bond lengths during the electron transfer. These concomitant phenomena uncovered in first-principle calculations characterize the essential equilibrium of the OEC between the state evolution and stability that forms a ground of the dynamic OEC cycles.

I. INTRODUCTION

The photosynthesis plays a crucial role in producing the biochemical energy to sustain the Earth's biological cycle. In converting the solar energy into the biochemical energy, the photosystem needs a carousel of electrons eventually from the water oxidation. Water oxidation is thus a fundamental reaction that is catalyzed at the oxygen evolving complex (OEC) in photosystem II (PSII) [1–5]. The whole catalytic process has long been thought to experience five redox reactions in a closed cycle, dubbed Kok's cycle (S_i , $i=0, \dots, 4$) [6], driven by the photoelectric hole at the PSII reaction centre, P_{680} [7], whereas its complete understanding remains challenging and a hot frontier.

In recent decade, the striking advances have arisen mainly from the measurements of the structures of S_i states using the high-resolution X-ray diffraction of the crystalized photosystems since the identification of the S_1 state structure in 2011 [8]. From then on, a series of experiments have progressively performed to identify the structures of S_2 and S_3 states [9–16]. Though the structure of S_4 state remains elusive, latest detection using serial femtosecond X-ray crystallography identified the presence of this intermediate on the time sequence of the evolution [17]. Another annual progress involving the S_4 state and subsequent oxygen radical identification was made strikingly upon the microsecond infrared spectroscopy of various vibration modes of protonated carboxylate sidechains [18]. The two different experiments provide complementary information on the S_4 state and the mechanism of the O_2 formation, but the characteristic time scale of events remains rather differ-

ent in these identifications. In addition to the structures of five S_i states, more information is indeed involved in the OEC reactions that include more intermediates associated with redox processes, deprotonations, water insertions and splitting, and the site-directed ionic interactions as well [5, 19].

For the supercomplex system that features multiple intermediates and piecewise evolution processes, in pursuit of simplicity is a natural strategy implemented not only in search of underlying laws but also with appropriately chosen systems. Therefore, this work focuses on the relatively simple evolutions between S_0 and S_2 prior to the water insertion and dissociation. The underlying laws for the evolutions of $S_0 \sim S_2$ can be used to understand the more involved subsequent state evolutions including the pending S_4 state. In particular, the evolutions of $S_0 \rightarrow S_1$ and $S_3 \rightarrow S_4$ are equally characteristic of the transfer of an electron and a proton. The state evolution is primarily started by the photoelectric hole that provides a Coulomb attraction to induce a serial electron transfer through the tyrosine residue (Tyr161) [20–22]. Physically, the polarization effect arising from the photoelectric hole and transferring electrons modifies the gradient of the electric potential that is responsible for the spin-orbit motions in atoms and molecules. In our previous work [23], we employed the spin flips of Mn atoms as a marker to trace the intermediates and evolution pathways of the OEC states in the dynamical polarization fields. In this work, we perform a more intensive and quantitative study on the polarization effects on the state evolutions. In particular, the emphases are placed on the evolution of the electron density of the states (DOS) and the coupling between the proton and electron transfers. In fact, the relationship between electron and proton transfers during the state evolutions is largely subject to a hot issue, whose elucidation remains rather scarce in the literature [24–29]. It was pointed out that the Tyr161 oxidation is accompa-

* wzjiang@seu.edu.cn

nied by the deprotonation to form a neutral radical with the rearrangement of the hydrogen bonding network and that the proton migrates back with a cooperative electron transfer from the CaMn_4O_5 [21, 30, 31]. Also, the electron loss in CaMn_4O_5 was found to be followed by a concomitant proton release from the water molecule W1 to Asp61 [30, 32]. These findings lead naturally to the question of how the proton and electron transfers couple in the evolution.

As the evolutions of S_0-S_2 are characterized mainly by electron transfers in the redox reactions of the CaMn_4O_5 cluster, concomitant changes are weaved by the shift of the local Coulomb field, the spin flips of Mn atoms, and propagated wrinkles in the electron density of states (DOS) near the Fermi surface. Using the density functional theory, we will search for the characteristic phenomenologies among these changes during the evolutions from S_0 to S_2 through S_1 . We will find that the characteristic phenomenologies can serve as the precursor to reveal the underlying physics of the water oxidation cycle.

The remainder of the paper is organized as follows. In Sec. II, we specify the model and methods of the density functional simulations. The results and discussion are presented in Sec. III, where we highlight the evolution of the electron DOS and the quantitative variations in characteristic bond lengths and oxidation states of Mn atoms in the electron transfer. At last, a brief summary is given in Sec. IV.

II. COMPUTATIONAL METHODS

We perform the spin-polarized all-electron density functional simulations with the DMol³ package in the Materials Studio of Accelrys Inc. The OEC system in the simulation is a 112-atom configuration whose schematic diagram in Fig. 1 is intercepted from the XRD crystal data obtained at 1.9 Å resolution [8]. In the geometric optimization process, we adopt the B3LYP hybrid functional [33–36]. The dynamic process of the electron transfer to the hole at Tyr161 induced by the polarization field is simulated by setting a point charge of the hole with 1.0e at Tyr161 and increasing the equivalent charge of the transferring electron placed at the fixed distance of 2 Å away from Ca atom of CaMn_4O_5 on the line connecting to the O atom of Tyr161. The fractional equivalent charge such as -0.1~ -0.9e is placed to simulate the distance-dependent Coulomb potential in a gradual transfer process of the electron. The effect of the position of the transferring electron is further verified by moving the equivalent charge of -0.9e to the position at a distance of 4 Å away from the Ca atom of CaMn_4O_5 , which is closer to the hole for further hole-electron recombination. In the simulation, the constraint of the charge conservation is imposed on the whole system. More details can be referred to Ref. [23].

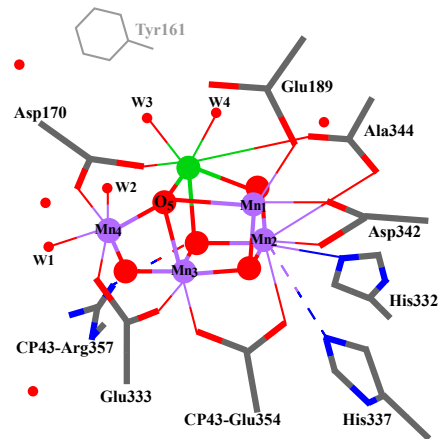


FIG. 1. Geometric model schematic diagram of the OEC CaMn_4O_5 , along with surrounding ligated amino acid residues. While hydrogen atoms are omitted for clarity, the Tyr161 outside of the model is sketched. The atoms of the CaMn_4O_5 are represented by spheres in different colors: Mn, Ca, and O atoms in purple, green, and red respectively. The ligand atoms are represented by various solid lines with grey, red, and blue colors denoting C, O, and N atoms, respectively.

III. RESULTS AND DISCUSSION

The evolutions from S_0 to S_2 primarily involve the transfer of electrons and protons from the CaMn_4O_5 , while the electron transfer fulfills at the hole-electron recombination. The dynamic electron transfer is associated with the variations in the bond valence and polarization field. Hence, elucidating the dynamic electron transfer can detail the animated evolution of CaMn_4O_5 and extract the characteristic phenomena in the presence of the varying polarization field. For $S_0\sim S_2$ states, the oxidation states of $\text{Mn}_1\sim\text{Mn}_4$ are reproduced to be S_0 (III, IV, III, III), S_1 (III, IV, IV, III), S_2 -open (III, IV, IV, IV), and S_2 -closed (IV, IV, IV, III), with the spin configurations of $\text{Mn}_1\sim\text{Mn}_4$ being $\uparrow\downarrow\uparrow\downarrow$, $\uparrow\downarrow\downarrow\uparrow$, $\uparrow\downarrow\downarrow\uparrow$, and $\uparrow\uparrow\downarrow$, respectively [1, 37].

When the hole polarization field switches on after the oxidation of Tyr161, the Mn spin configuration of the S_0 state flips from $\uparrow\downarrow\uparrow\downarrow$ to $\uparrow\downarrow\downarrow\uparrow$, accompanied by an increase in the total energy of the system. In response to the hole polarization field, the system undergoes an excitation to an intermediate for subsequent electron transfer. The similar spin flip of the S_1 state occurs in the hole polarization field with the Mn spin configuration to $\uparrow\uparrow\downarrow$. Then, the candidate Mn atom of the electron donor loses one electron for recombination with the hole at Tyr161.

In the process of the electron transfer from the OEC, the effective charge of the transferring electron is set to vary from -0.1e to -0.9e at a site 2 Å away from the Ca atom of CaMn_4O_5 on the line connecting to the O atom of Tyr161. During this process, we can observe that the spin configuration of Mn atoms undergoes some intermediate configurations and flip exactly to that of the next

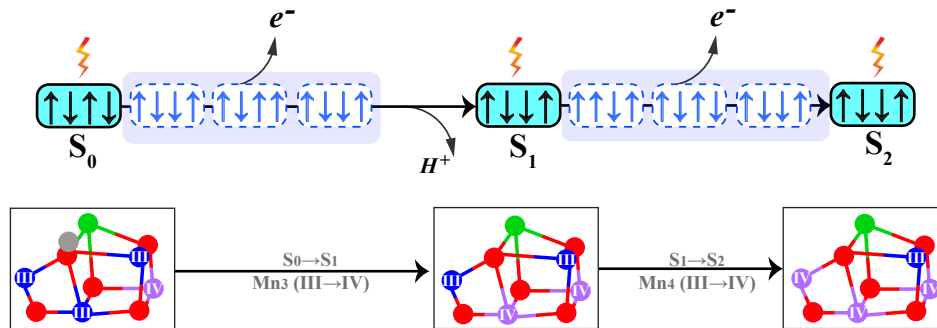


FIG. 2. Evolutions of spin configurations and oxidation states of Mn atoms for $S_0 \sim S_2$. The spins in solid and dashed boxes are for the S_i and intermediate states, respectively. In the second row, the Mn atoms are marked with oxidation states (III and IV), and Ca, O, and H atoms are denoted by green, red, and grey spheres, respectively.

S state, see Fig. 2. In the evolution from S_0 to S_1 , the Mn spin configuration ultimately changes to $\uparrow\downarrow\downarrow\uparrow$ after going through $\uparrow\downarrow\uparrow\uparrow$. When the released electron moves closer to Tyr161 at a distance of 4 Å away from the Ca atom of the CaMn_4O_5 , the spin configuration of Mn atoms remains unchanged. The subsequent proton removal also does not alter the Mn spin configuration of $\uparrow\downarrow\downarrow\uparrow$, which then becomes the spin configuration of the S_1 state. Similar spin flips are observed in the process of an electron transfer from the OEC of the S_1 state, as shown in Fig. 2. After the electron transfer, the spin configuration shifts to that of the S_2 -open. The occurrence of the spin flips of Mn atoms is attributed to the electron transfer and the resulting shift in the Coulomb field induced by the hole polarization, while the change in the Coulomb field modifies the spin-orbit motions due to the spin-orbital coupling $\xi(r) = \vec{\sigma} \cdot \hat{\mathbf{L}} / (2m_e^2rc^2)dV/dr$ [23]. The spin flips elaborate the electron transfer process and can serve as an indicative marker for the pivotal OEC evolution driven by the hole polarization.

Shown in Fig. 2 is also the variation in the bond valence of Mn atom that represents for an electron transmission from below the Fermi surface to the liberation of the Coulomb binding. This demonstrates the necessity to examine the variation in the density of states (DOS) especially near the Fermi surface in the process of the electron transfer. Figure 3 shows the variation in the partial DOS (PDOS) of s , p and d orbitals for the atoms of $\text{Mn}_1 \sim \text{Mn}_4$ with increasing the effective charge of the transferring electron at the specified position during the evolution from S_0 to S_1 . It is found that in the S_0 state the value of the Mn_3 DOS of the d orbital is significant at the site sufficiently near Fermi surface. We can observe from the third row of Fig. 3 that the Mn_3 DOS of the d orbital comes across the Fermi surface to form a small separate peak that blends into the bumps above the Fermi surface in a process where the electron transfer is simulated by placing the effective charge of -0.1, -0.5 and -0.9e at the site specified above, respectively. Compared with the sluggish changes in the PDOS of other Mn atoms, it clearly suggests that Mn_3 is the electron donor during

the evolution from S_0 to S_1 , which is actually in accord with the variation of the Mn oxidation state. During the electron transfer until its fulfillment, the PDOS boundaries of Mn atoms below the Fermi surface experience more or less a contraction inwards to keep the electron distributions better bound. This leads to a temporary stability of the OEC in the dynamical OEC evolution prior to the proton transfer. The proton transfer pushes the PDOS of Mn atoms outwards and especially brings the Mn_4 PDOS to scrape over the Fermi surface. This gives the opportunity and vigor for another ignition.

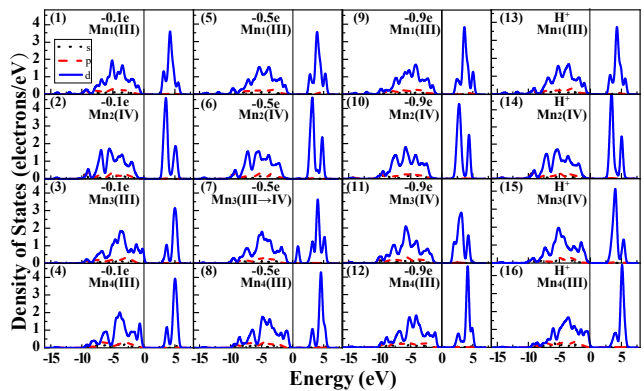


FIG. 3. The PDOS of s , p and d orbitals of $\text{Mn}_1 \sim \text{Mn}_4$ during $S_0 \rightarrow S_1$. Column panels are with effective charge of -0.1, -0.5 and -0.9 e of the transferring electron and with the proton transfer, respectively. The vertical line represents the Fermi surface.

As another light flash breaks the tranquility, the photoelectric hole is recreated to drive the evolution from the S_1 to S_2 state. Similar variations in the Mn PDOS arise from the electron transmission from below the Fermi surface. At this time, it is the Mn_4 PDOS that shows the animation from coming across the Fermi surface to undergoing the splitting and blending into high-level distributions well above the Fermi surface, as shown clearly in Fig. 4. The characteristic variation of the Mn_4 PDOS near the Fermi surface is consistent with the shift of its

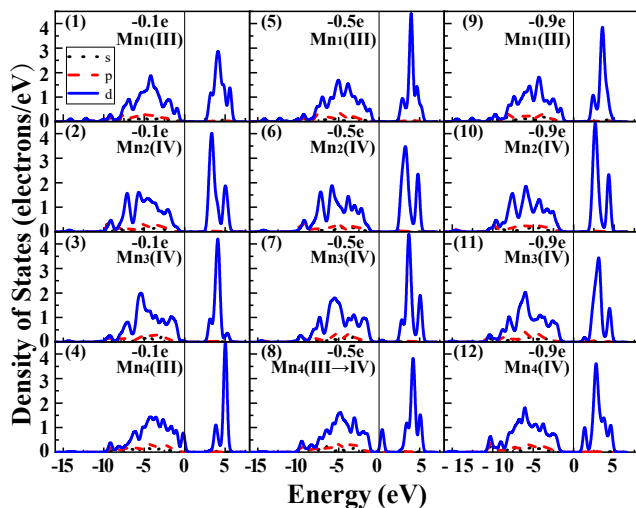


FIG. 4. The same as in Fig. 3 but for $S_1 \rightarrow S_2$ without proton transfer.

oxidation state from the third to fourth valence. Similar to the evolution from the S_0 to S_1 state, the release of electron seems to stabilize the catalyst cluster. This establishes the essential equilibration between the dynamic evolution and the state stability that forms a necessary foundation for the precessing OEC cycle. Moreover, it should be stressed that the electron transfer here is correlated with the preceding proton transfer with which the hydrogen bonding network is associated tightly [38].

During the electron transfer, the PDOS of all Mn atoms in the Fermi sea is observed to undergo some rearrangements. As a result, the concomitant microscopic changes are also found in the oxidation states and spin configurations of Mn atoms, as shown in Fig. 5. Here, the Mn oxidation state is calculated from the bond valence sum (BVS) formula $S = \sum \exp(R_0 - R_{ij})/B_0$, where R_{ij} represents each bond length between the Mn and surrounding O or N atoms, and other relevant parameters are taken as $B_0=0.37$, $R_0(\text{Mn-O})=1.750 \text{ \AA}$, and $R_0(\text{Mn-N})=1.822 \text{ \AA}$ [39]. It can be observed from Fig. 5a and b that the variations in the oxidation states of the candidate Mn atoms of the electron donor are almost linearly correlated with the effective charge of the transferring electron, while the oxidation states of other Mn atoms remain nearly unchanged. Specifically, with the effective charge of the transferring electron varying from -0.1 to $-0.9 e$, the Mn_3 oxidation state gradually changes from about 2.9 to 3.7 in $S_0 \rightarrow S_1$ and Mn_4 changes from 2.8 to 3.7 in $S_1 \rightarrow S_2$, representing a valence change from III to IV. During the electron transfer in the polarization field, the spin flips of Mn atoms may occur with the changes of Mn oxidation states. Depicted in Fig. 5c and d are the Mulliken spin populations of Mn atoms that give the number of unpaired electrons around Mn and the spin orientations. The positive and negative values correspond to up and down spin orientations, respectively. The reduction of the Mn_3 and Mn_4 spin populations from

4 to 3 in $S_0 \rightarrow S_1$ and $S_1 \rightarrow S_2$ accords with the shift of their oxidation states from III to IV for the electron transfer. It can be seen from Fig. 5c and d that some intermediate states are produced with the spin flips of Mn atoms during the electron transfer. Especially, multiple flips of the Mn spin orientations take place in the transfer process of $S_1 \rightarrow S_2$. With a succession of intermediate states in the varying polarization field, the OEC states (S_0 , S_1) evolve to the next state with the electronic and geometric structures consistent with those from the measurements and theoretical computations [40–47].

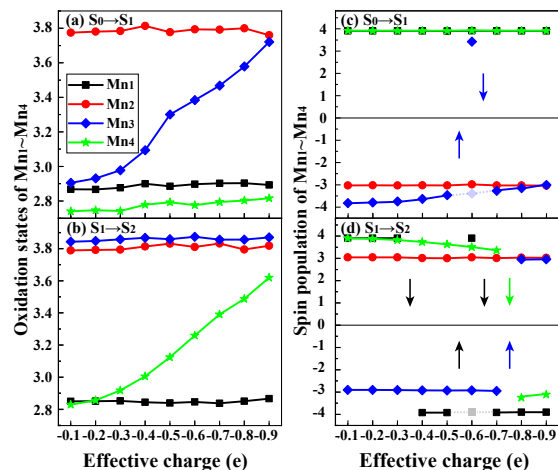


FIG. 5. Variations of $\text{Mn}_1 \sim \text{Mn}_4$ oxidation states (a) and (b), and their Mulliken spin population (c) and (d). The effective charge of the transferring electron varies from -0.1 to $-0.9 e$ with the polarization field imposed. The arrows in (c) and (d) represent the flip of spin orientation.

In the dynamical evolution, the above microscopic quantum shifts are also accompanied by the change in the phenomenological geometrical structure. Figure 6 displays the variations of Mn-O₅ and Mn-Mn bond length during the electron transfer under the polarization field. In Fig. 6a and b, the variations of the bond lengths during the electron transfer of $S_0 \rightarrow S_1$ and $S_1 \rightarrow S_2$ are relative to those of S_0 and S_1 states, respectively. Positive and negative values stand for the elongation and shortening of bond lengths, respectively. It can be observed that the alteration in Mn-O bond lengths is more appealing due to the attraction between them, while the less altered Mn-Mn distances suggest that the S_i structures are rather stable during the electron transfer. In Fig. 6a, the main change is observed to be the considerable shortening of the $\text{Mn}_3\text{-O}_5$ bond length that is approximately 0.35 \AA with the effective charge of the transferring electron varying from -0.1 to $-0.9 e$ during the electron transfer from S_0 to S_1 state. The large shortening arises from the electron loss of Mn_3 that gives rise to a stronger attraction between Mn_3 and O_5 .

In the evolution of $S_1 \rightarrow S_2$, the $\text{Mn}_1\text{-O}_5$ length shows an overall trend of elongation, while the $\text{Mn}_4\text{-O}_5$ length displays the opposite trend of shortening, as the effective

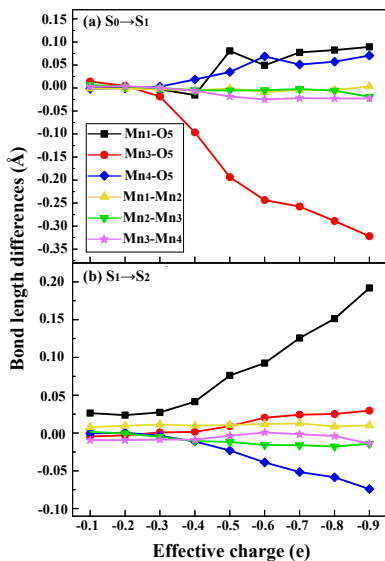


FIG. 6. Variations of Mn-O₅ and Mn-Mn bond lengths. In (a) and (b), the results are relative to those of the S₀ and S₁ states, respectively. The effective charge of the transferring electron varies from -0.1 to -0.9 e with the polarization field imposed.

charge of the transferring electron varies from -0.1 to -0.9 e, see Fig. 6b. The shortening of the Mn₄-O₅ bond length is attributed to the enhanced attraction between Mn₄ and O₅ due to the electron loss of Mn₄. In contrast, the attraction between Mn₁ and O₅ is weakened to cause the elongation of the bond length. Specifically, the Mn₁-O₅ length increases by about 0.2 Å throughout the electron transfer process, corresponding to the Mn₁-O₅ bond length of 2.901 and 3.092 Å in S₁ and S₂-open state, respectively. The active variation of the Mn₁-O₅ and Mn₄-O₅ bonds suggests the existence of the live domain in the OEC structure. Actually, the counteraction between the Mn₁-O₅ and Mn₄-O₅ bondings offers support for the existence of two structures that are characteristic of the commodious space with the elongated

bond length of Mn₁-O₅ and Mn₄-O₅, called S₂-open and S₂-closed [44], respectively.

IV. SUMMARY

In this work, we investigate the OEC evolutions during S₀ ~ S₂ to reveal the animation and mechanisms therein by virtue of the characteristic signals with the density functional simulations. The electron transfer is eventually driven by the hole polarization, whereas a direct evidence of the correlation with the proton transfer is revealed in the state evolution during which the electron donor Mn atom is readily prepared by the preceding proton transfer. The characteristic shift of the Mn PDOS near the Fermi surface is found to correlate simultaneously with the variations in the Mn oxidation states and spin flips, together with the change in the geometric structure. These concurrent events consist of a collection of the characteristic signals for the state evolution. In particular, the spin flips of Mn atoms, consistent with variation of the Mulliken spin populations, can point exactly to the spin configuration of the next S_i state after undergoing some intermediates during electron transfer. Importantly, the stability of the OEC arising from the electron transfer brings the rhythm in the theme of the dynamical evolution that is necessary for the unceasing OEC cycle. Our findings will play an instructive role in unveiling the pending S₄ state and revealing more underlying physics for the water oxidation cycle.

ACKNOWLEDGEMENTS

This work was supported in part by the National Natural Science Foundation of China under Grants No. 11775049 and No. 12375112. The Big Data Computing Center of Southeast University is acknowledged for providing the facility support for the partial numerical calculations of this work.

- [1] J.-R. Shen, *Annual review of plant biology* **66**, 23 (2015).
- [2] D. J. Vinyard and G. W. Brudvig, *Annual review of physical chemistry* **68**, 101 (2017).
- [3] Q.-F. Chen, Y.-H. Guo, Y.-H. Yu, and M.-T. Zhang, *Coordination Chemistry Reviews* **448**, 214164 (2021).
- [4] M. Shamsipur and A. Pashabadi, *Coordination Chemistry Reviews* **374**, 153 (2018).
- [5] C. F. Yocum, *Photosynthesis Research* **152**, 97 (2022).
- [6] B. Kok, B. Forbush, and M. McGloin, *Photochemistry and Photobiology* **11**, 457 (1970).
- [7] M. M. Najafpour, I. Zaharieva, Z. Zand, S. M. Hosseini, M. Kouzmanova, M. Holyńska, I. Tranca, A. W. Larkum, J.-R. Shen, and S. I. Allakhverdiev, *Coordination Chemistry Reviews* **409**, 213183 (2020).
- [8] Y. Umena, K. Kawakami, J.-R. Shen, and N. Kamiya, *Nature* **473**, 55 (2011).
- [9] R. Pokhrel and G. W. Brudvig, *Physical Chemistry Chemical Physics* **16**, 11812 (2014).
- [10] N. Cox, M. Retegan, F. Neese, D. A. Pantazis, A. Bousac, and W. Lubitz, *Science* **345**, 804 (2014).
- [11] I. D. Young, M. Ibrahim, R. Chatterjee, S. Gul, F. D. Fuller, S. Koroidov, A. S. Brewster, R. Tran, R. Alonso-Mori, T. Kroll, *et al.*, *Nature* **540**, 453 (2016).
- [12] M. Suga, F. Akita, M. Sugahara, M. Kubo, Y. Nakajima, T. Nakane, K. Yamashita, Y. Umena, M. Nakabayashi, T. Yamane, *et al.*, *Nature* **543**, 131 (2017).
- [13] J. Kern, R. Chatterjee, I. D. Young, F. D. Fuller, L. Lassalle, M. Ibrahim, S. Gul, T. Fransson, A. S. Brewster, R. Alonso-Mori, *et al.*, *Nature* **563**, 421 (2018).

- [14] A. J. Wilson and P. K. Jain, *Journal of the American Chemical Society* **140**, 5853 (2018).
- [15] M. Ibrahim, T. Fransson, R. Chatterjee, M. H. Cheah, R. Hussein, L. Lassalle, K. D. Sutherlin, I. D. Young, F. D. Fuller, S. Gul, *et al.*, *Proceedings of the National Academy of Sciences* **117**, 12624 (2020).
- [16] R. Hussein, M. Ibrahim, A. Bhowmick, P. S. Simon, R. Chatterjee, L. Lassalle, M. Doyle, I. Bogacz, I.-S. Kim, M. H. Cheah, *et al.*, *Nature communications* **12**, 6531 (2021).
- [17] A. Bhowmick, R. Hussein, I. Bogacz, P. S. Simon, M. Ibrahim, R. Chatterjee, M. D. Doyle, M. H. Cheah, T. Fransson, P. Chernev, *et al.*, *Nature* **617**, 629 (2023).
- [18] P. Greife, M. Schönborn, M. Capone, R. Assunção, D. Narzi, L. Guidoni, and H. Dau, *Nature* **617**, 623 (2023).
- [19] A. P. Avramov, H. J. Hwang, and R. L. Burnap, *Proceedings of the National Academy of Sciences* **117**, 28036 (2020).
- [20] T. J. Wydrzynski, K. Satoh, and J. A. Freeman, *Photosystem II: the light-driven water: plastoquinone oxidoreductase*, Vol. 22 (Springer, 2005).
- [21] S. Styring, J. Sjöholm, and F. Mamedov, *Biochimica et Biophysica Acta (BBA)-Bioenergetics* **1817**, 76 (2012).
- [22] B. A. Barry and G. T. Babcock, *Proceedings of the National Academy of Sciences* **84**, 7099 (1987).
- [23] P.-Y. Huo, W.-Z. Jiang, R.-Y. Yang, and X.-R. Zhang, *Phys. Rev. Appl.* **21**, 024024 (2024).
- [24] T. Shimizu, M. Sugiura, and T. Noguchi, *The Journal of Physical Chemistry B* **122**, 9460 (2018).
- [25] H. Dau and M. Haumann, *Biochimica et Biophysica Acta (BBA)-Bioenergetics* **1767**, 472 (2007).
- [26] B. A. Barry, *Biochimica et Biophysica Acta (BBA)-Bioenergetics* **1847**, 46 (2015).
- [27] C. J. Gagliardi, A. K. Vannucci, J. J. Concepcion, Z. Chen, and T. J. Meyer, *Energy & Environmental Science* **5**, 7704 (2012).
- [28] G. Renger, *Biochimica et Biophysica Acta (BBA)-Bioenergetics* **1655**, 195 (2004).
- [29] I. Zaharieva, H. Dau, and M. Haumann, *Biochemistry* **55**, 6996 (2016).
- [30] S. Nakamura, M. Capone, D. Narzi, and L. Guidoni, *Physical Chemistry Chemical Physics* **22**, 273 (2020).
- [31] S. Nakamura, R. Nagao, R. Takahashi, and T. Noguchi, *Biochemistry* **53**, 3131 (2014).
- [32] D. Narzi, D. Bovi, and L. Guidoni, *Proceedings of the National Academy of Sciences* **111**, 8723 (2014).
- [33] A. D. Becke, *The Journal of chemical physics* **96**, 2155 (1992).
- [34] C. Lee, W. Yang, and R. G. Parr, *Physical review B* **37**, 785 (1988).
- [35] S. H. Vosko, L. Wilk, and M. Nusair, *Canadian Journal of physics* **58**, 1200 (1980).
- [36] P. J. Stephens, F. J. Devlin, C. F. Chabalowski, and M. J. Frisch, *The Journal of physical chemistry* **98**, 11623 (1994).
- [37] V. Krewald, M. Retegan, F. Neese, W. Lubitz, D. A. Pantazis, and N. Cox, *Inorganic chemistry* **55**, 488 (2016).
- [38] D. A. Horke, H. M. Watts, A. D. Smith, E. Jager, E. Springate, O. Alexander, C. Cacho, R. T. Chapman, and R. S. Minns, *Phys. Rev. Lett.* **117**, 163002 (2016).
- [39] W. Liu and H. H. Thorp, *Inorganic Chemistry* **32**, 4102 (1993).
- [40] R. Pal, C. F. Negre, L. Vogt, R. Pokhrel, M. Z. Ertem, G. W. Brudvig, and V. S. Batista, *Biochemistry* **52**, 7703 (2013).
- [41] P. E. Siegbahn, *Biochimica et Biophysica Acta (BBA)-Bioenergetics* **1827**, 1003 (2013).
- [42] D. Koulougliotis, D. J. Hirsh, and G. W. Brudvig, *Journal of the American Chemical Society* **114**, 8322 (1992).
- [43] M. Askerka, D. J. Vinyard, G. W. Brudvig, and V. S. Batista, *Biochemistry* **54**, 5783 (2015).
- [44] D. A. Pantazis, W. Ames, N. Cox, W. Lubitz, and F. Neese, *Angewandte Chemie International Edition* **51**, 9935 (2012).
- [45] J. Zimmermann and A. Rutherford, *Biochemistry* **25**, 4609 (1986).
- [46] A. Haddy, K. Lakshmi, G. W. Brudvig, and H. A. Frank, *Biophysical journal* **87**, 2885 (2004).
- [47] A. V. Astashkin, Y. Kodera, and A. Kawamori, *Journal of Magnetic Resonance, Series B* **105**, 113 (1994).